C. R. Chimie 20 (2017) 1017–1025

Contents lists available at ScienceDirect

Comptes Rendus Chimie

www.sciencedirect.com

Full paper/Mémoire

Mesostructured silica–titania composites for improved oxytetracycline delivery systems

Doina Georgescu [a], Ana-Maria Brezoiu [a], Raul-Augustin Mitran [b], Daniela Berger [a], Cristian Matei [a, *], Bogdan Negreanu-Pirjol [c]

[a] University "Politehnica" of Bucharest, Department of Inorganic Chemistry, Physical–Chemistry and Electrochemistry, Polizu Street no. 1–7, Bucharest 011061, Romania
[b] "Ilie Murgulescu" Institute of Physical–Chemistry, Romanian Academy, 202 Splaiul Independentei, Bucharest 060021, Romania
[c] Ovidius University of Constanta, Department of Pharmaceutical Sciences, Aleea Universitatii No. 1, Constanta 900470, Romania

ARTICLE INFO

Article history:
Received 2 July 2017
Accepted 26 September 2017
Available online 1 November 2017

Keywords:
Mesoporous materials
Silica–titania composite
Antibiotic
SBA-15
Drug delivery systems

ABSTRACT

Mesoporous silica and titania are biocompatible materials and could be used as carriers for various drugs due to their excellent hosting capacity. Here, we report studies on the preparation of oxytetracycline delivery systems containing various mesostructured silica–titania SBA-15–type supports with up to 30 mol % titania to establish the influence of structural, textural, and support composition on the oxytetracycline release profile. The antibiotic was loaded into the support mesochannels by the incipient wetness impregnation method. The drug delivery profiles obtained in phosphate-buffered saline showed that the increase in titania content in the mesoporous support slowed down the release kinetics. The oxytetracycline-loaded materials demonstrated good antimicrobial activity against *Staphylococcus aureus* ATCC 25923 strain.

1. Introduction

Many research efforts are underway to enhance the effectiveness of treatment with antibiotics because the incidence of infections with resistant strains has significantly increased. One way to improve the treatment efficiency is the design of new pharmaceutical formulations containing the antibiotics already in use, aiming to minimize the adverse effects and control the drug release to ensure an optimal dose.

In the past few years, mesoporous silica, especially MCM-41 (Mobil Composition of Matter no. 41) and SBA-15 (Santa Barbara Amorphous), both presenting an ordered hexagonal pore array, has received an increased interest for hosting and further controlling release of various active pharmaceutical ingredients due to its outstanding properties as tunable particles size and pore diameter between 2 and 10 nm, high specific surface area up to 1200 m^2/g, and total pore volume up to 1.5 cm^3/g allowing the accommodation of a high quantity of drug molecules. Moreover, the silanol-containing surface can be involved in bonding of different organic moieties via functionalization, offering the possibility to modulate the interactions between biologically active molecules and silica [1–7].

For drug delivery purposes, mesoporous titania nanoparticles were studied since 2012, when they were designed as support for ibuprofen [8]. Unlike silica, mesoporous titania exhibits lower porosity (up to 200 m^2/g and 0.4 cm^3/g) and smaller concentration of hydroxyl groups on their surface, but it could interact with drug molecules through donor–acceptor bonds. Mesoporous titania films coating titanium implants are used as antibiotic reservoirs for local delivery to enhance osteointegration [9,10]. Recently, a superior hemocompatibility of titania nanoparticles compared to mesoporous silica was demonstrated [11].

* Corresponding author.
E-mail address: cristi_matei@yahoo.com (C. Matei).

https://doi.org/10.1016/j.crci.2017.09.006
1631-0748/

To date, mesoporous silica–titania composites have been studied for their synergic properties, especially as photocatalysts [12–15]. With respect to their preparation, silica–titania composites were obtained by the sol–gel method through embedding anatase nanoparticles into the silica phase [16,17] or by loading a titania precursor solution into previously prepared MCM-41 through incipient wetness impregnation [18,19].

Recently, silica–titania composites were also used for biomedical applications. For instance, by replacing silicon atoms with titanium in the SBA-15 silica matrix a versatile carrier for either water-soluble or insoluble drug molecules was reported. The presence of titanium atoms into the silica framework at 4.2 μmol/g concentration decreases the negative surface charge of a silica matrix and thus negative-charged drug molecules can be loaded into the Ti-modified silica mesopores [20]. It was also reported the incorporation of vancomycin and farnesol into silica thin film, which coated the titanium alloy rod implant, for local codelivery and thus it can avoid any further surgery [21]. Titania–silica composites with MCM-41 structure were explored as vehicles for encapsulation of a new antibacterial agent, izohidrafural, and the resulted drug-loaded materials exhibited superior bactericidal activity against *Gram-negative* strains [22].

Oxytetracycline is a broad-spectrum antimicrobial agent, which belongs to the tetracycline class and it is used in human and veterinary medicine, as well as in animal feed. Because of its extensively usage in the animal feed, there is a risk for humans in developing bacterial resistance or allergies. One way to overcome this aspect is the use of polymeric or inorganic nanoparticles as vehicles for obtaining efficient drug delivery systems (DDSs). It is difficult to incorporate oxytetracycline molecules into a carrier and to control its release kinetics because of its high water solubility. Therefore, there are only few reports about the encapsulation of tetracycline class of antibiotics to obtain DDS. Recently, Hashemikia et al. [23] by comparing two mesostructured silica materials, pristine SBA-15 and aminopropyl functionalized SBA-15 as supports for tetracycline, obtained a slower antibiotic release rate for modified silica carrier than for SBA-15. An oxytetracycline delivery system containing microfibrillated cellulose as vehicle that allowed a drug sustained release and preserved its antimicrobial activity was recently reported [24]. Also, poly(hydroxyethylmethacrylate) as oxytetracycline carrier was evaluated and studies on in vivo release in gastrointestinal environment and toxicity assays on mice model recommended this DDS for oral therapy [25]. To obtain a lower burst effect of oxytetracycline release profile, Kleinubing et al. [26] developed a controlled delivery system by coating alginate/chitosan microparticles with acryl-EZE MP, an enteric coating system, based on Eudragit polymer.

Herein, we report studies on the synthesis of mesostructured silica–titania SBA-15–type composites with up to 30 mol % titania by a sol–gel technique combined with a hydrothermal treatment, which were further explored as carriers for oxytetracycline. Previously, we reported that oxytetracycline-loaded into MCM-41 silica and aluminosilicate mesopores [27] or silica–ceria MCM-41–type composites [28] presented a burst release effect followed by a sustained delivery from MCM-41–type support and exhibited a good antibacterial activity against five clinical isolates of *Staphylococcus aureus* strains. [27] By modification of the SBA-15 matrix through the introduction of titania we expect to enhance the interactions between drug molecules and mesoporous silica–titania composites leading to a slower antibiotic release kinetics.

2. Experimental section

2.1. Materials and chemical reagents

Tetraethyl orthosilicate (TEOS, Fluka), titanium(IV) isopropoxide (≥97%, Aldrich), poly(ethylene glycol)-*block*-poly(propylene glycol)-*block*-poly(ethylene glycol), Mw = 5800 (Pluronic, P123, Aldrich), hydrochloric acid 37% (Sigma–Aldrich), sodium chloride (≥99%, Sigma), absolute ethanol (Sigma–Aldrich), potassium dihydrogen phosphate (KH_2PO_4, Merck), sodium hydrogen phosphate (Na_2HPO_4, Sigma–Aldrich), and oxytetracycline hydrochloride (Sigma) were used as received without further purification. Ultrapure deionized water (Millipore Direct-Q3UV water systems with Biopack UF cartridge) was used in all experiments.

2.2. Synthesis of mesoporous carriers

The mesostructured silica–titania composites with up to 30 mol % titania and one-dimensional pore array, characteristic for SBA-15–type silica, were obtained by the sol–gel method assisted by hydrothermal treatment using TEOS and titanium oxydichloride as silica and titania precursors, respectively, in the presence of triblock copolymer, Pluronic P123, as a structure-directing agent. The silica–titania supports for oxytetracycline were compared with a SBA-15 silica material. Titanium oxydichloride was freshly prepared from titanium(IV) isopropoxide and concentrated hydrochloric acid according to the literature data [29]. In brief, 5 mL titanium(IV) isopropoxide was added dropwise under magnetic stirring to 9.4 mL concentrated hydrochloric acid at 0 °C and kept at this temperature for 1 h.

For the synthesis of silica–titania composites, 1.05 g Pluronic P123 was dissolved in 52 mL of water in which 0.77 g NaCl was previously added, at room temperature. Then, the corresponding volume of TEOS was poured into the polymer solution at room temperature, under magnetic stirring, followed by the addition of titanium oxydichloride. The total amount of a TEOS and $TiOCl_2$ mixture was 0.0132 mol with Si/Ti molar ratio values of 95.5/4.5, 90/10, 80/20, and 70/30, the synthesized silica–titania composites being labeled as Ti4.5SBA-15, Ti10SBA-15, Ti20SBA-15, and Ti30SBA-15. The reaction mixture was aged at 35 °C, 24 h, and then was transferred in a Teflon lined autoclave for the hydrothermal treatment performed at 100 °C, 48 h, under autogenerated pressure. After this, the solid was filtered off, intensively washed with water and ethanol, dried at room temperature, and calcined at 550 °C for 5 h.

SBA-15 silica support was prepared in the presence of triblock copolymer P123 as a structure-directing agent, in an aqueous slightly acidic solution, in a molar ratio of TEOS/

P123/H_2O/NaCl/HCl 1:0.014:218.9:1:0.32. The reaction mixture was first aged at 35 °C for 24 h and then hydrothermally treated in the same conditions as silica–titania composites. The solid was recovered by filtration and then was washed, dried at room temperature, and calcined at 550 °C for 5 h.

2.3. Obtaining the drug-loaded materials and in vitro release experiments

The oxytetracycline-loaded materials with a drug content of 25 or 33 wt% were obtained by the incipient wetness impregnation method using a concentrated aqueous solution of antibiotic. In brief, 100 mg mesoporous support was added to the corresponding volume of a freshly prepared oxytetracycline hydrochloride aqueous solution with a concentration of 100 mg/mL. The support and antibiotic solution were mixed for homogenization, and then the mixture was vacuum dried in dark conditions for 12 h.

The oxytetracycline release experiments were performed in 0.2 M phosphate-buffered saline (PBS) as simulated body fluid at 37 °C under magnetic stirring (150 rpm). An amount of drug-loaded material containing 12.5 mg antibiotic was added to 90 mL PBS. At predetermined time intervals, set amounts of simulated body fluid were withdrawn, diluted, and analyzed by UV–vis spectroscopy, using an Ocean Optics USB 4000 spectrophotometer, to determine the antibiotic release amount.

2.4. Material characterization

The mesoporous supports were characterized using small-angle X-ray diffraction (XRD) carried out on a Bruker B8 Discover diffractometer with Cu Kα radiation (λ = 1.5406 Å), with a scanning rate of 0.5°/min and a step of 0.02°. The wide-angle XRD patterns of mesoporous silica–titania composites and oxytetracycline-loaded materials were recorded using a Rigaku MiniFlex II diffractometer in 10°–70° and 6°–50°, respectively, 2θ range, and 2°/min scanning rate. The Fourier transform infrared (FTIR) spectra of carriers and oxytetracycline-loaded samples were recorded using a Bruker Tensor 27 spectrometer in the range of 4000–400 cm^{-1} (KBr pellet technique). The morphology of silica–titania composites was investigated by scanning electron microscopy (SEM) and transmission electron microscopy (TEM). SEM was performed using a Tescan Vega 3 LMH microscope coupled with an energy dispersive X-ray (EDX) spectrophotometer, and TEM was carried out on FEI Tecnai G2-F30S-Twin field-emission gun scanning transmission electron microscope operating at 300 kV. A drop of the mesoporous silica–titania alcoholic suspension was mounted on a holey carbon film copper grid allowing the solvent to evaporate at room temperature. Both carriers and oxytetracycline-loaded samples were investigated by N_2 adsorption/desorption isotherms performed at 77 K, using a Quantachrome Autosorb iQ_2 surface and porosity analyzer. Before analysis, the samples were outgassed under vacuum at 300 °C for 6 h in the case of inorganic matrices and at 35 °C for 17 h for drug-loaded samples. The pore size distribution curves of samples were determined by the Barrett–Joyner–Halenda (BJH) method, and the specific surface area values were estimated using the Brunauer–Emmett–Teller (BET) model in the relative pressure range of 0.05–0.25.

2.5. Antimicrobial activity assays

The antibacterial activity of oxytetracycline-loaded materials in comparison with that of the antibiotic alone was evaluated against three reference BioMérieux strains: *S. aureus* ATCC 25923, *Escherichia coli* ATCC 25922, and *Pseudomonas aeruginosa* ATCC 27853. The reference strains were grown overnight in tryptone soy broth (Sigma–Aldrich) diluted to 5×10^5 CFU/mL (0.5 McFarland density) and inoculated onto Mueller–Hinton Agar medium. Before any experiment, the organisms were subcultured in a fresh yeast nitrogen broth (Sigma–Aldrich) with 0.5% glucose (*p*-aminobenzoic acid, 200 μg/L; ammonium sulfate, 5 g/L; biotin, 2 μg/L; boric acid, 500 μg/L; calcium chloride, 0.1 g/L; and calcium pantothenate, 400 μg/L). The antimicrobial activity of drug-loaded samples was assessed by depositing weighed amounts of samples containing 1 mg of antibiotic on the surface of inoculated culture medium in sterile conditions to evidence the effect of prepared oxytetracycline-containing samples on the bacterial cultures. As positive control oxytetracycline hydrochloride powder was used. All experiments were performed in triplicate. The plates containing the microbial cultures treated with the samples were incubated at 37 °C for 24 h and then the growth inhibition zone diameter induced by the tested materials was measured.

3. Results and discussion

3.1. Supports and drug-loaded materials

The pristine SBA-15 silica and silica–titania composite materials were characterized by small- and wide-angle

Table 1
Structural and textural parameters of mesoporous carriers.

Sample	Ti content (mol %)	d_{100} (nm)	a_0 (nm)	Wt (nm)	S_{BET} (m^2/g)	d_{BJH}[a] (nm)	V_{pt}/V_p[b] (cm^3/g)	D_{200}[c] (nm)
SBA-15	0	10.960	12.655	4.515	997	8.14	1.49/1.34	–
Ti4.5SBA-15	4.5	11.005	12.707	6.437	959	6.27	1.29/1.10	12.5
Ti10SBA-15	10	11.170	12.898	6.078	1081	6.82	1.50/1.21	75.9
Ti20SBA-15	20	11.479	13.255	6.445	826	6.82	1.50/1.21	78
Ti30SBA-15	30	11.663	13.468	6.058	742	7.41	1.24/1.14	100

[a] Pore diameter determined from the desorption branch of isotherms.
[b] V_{pt}/V_p is the total pore volume including mesopores and macropores versus mesopore volume of pores with diameter less than 10 nm.
[c] TiO_2 crystallite size computed from (200) diffraction peak (2θ ~ 48°) of the anatase phase.

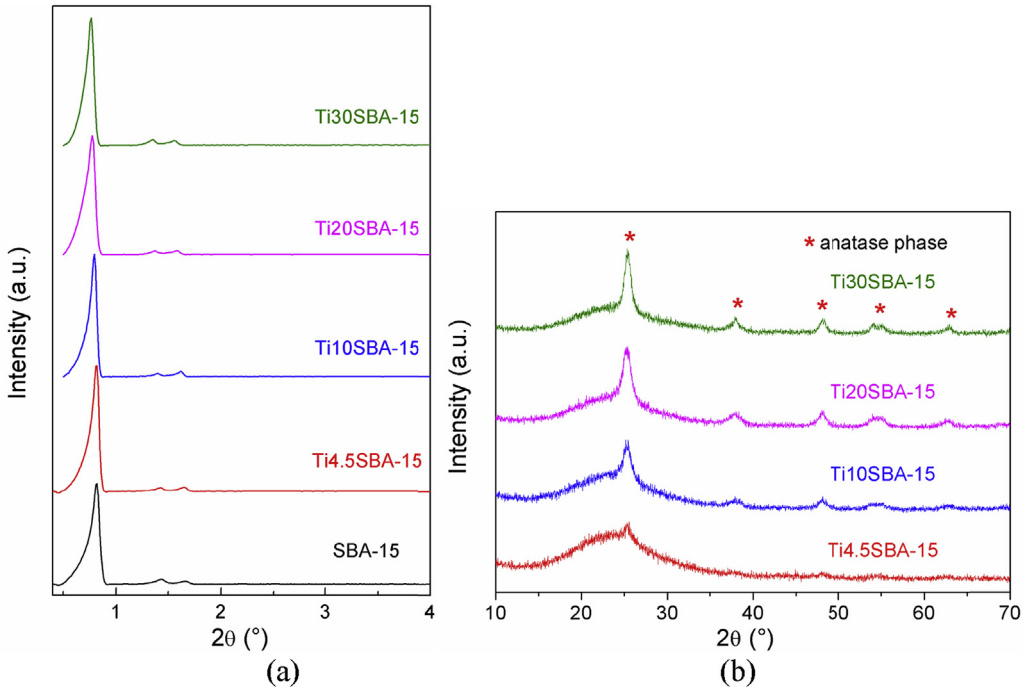

Fig. 1. Small-angle (a) and wide-angle (b) XRD patterns of mesoporous supports.

XRD, FTIR spectroscopy, SEM, TEM, and nitrogen adsorption–desorption isotherms.

The small-angle XRD patterns of all synthesized supports present three characteristic diffraction peaks corresponding to (10), (11), and (20) Bragg reflections of SBA-15–type materials, proving the formation of an ordered hexagonal pore array for all samples (Fig. 1a) The increase in titanium content led to the enlargement of a_0 lattice parameter (Table 1). The wide-angle XRD patterns of titania-containing samples show the diffraction peak characteristics for the anatase phase and the broad signal corresponding to the amorphous state of a silica network (Fig. 1b). The only exception is the Ti4.5SBA-15 sample for which the diffraction reflections of the anatase phase are hardly detectable, suggesting that titanium is mostly incorporated into the silica framework, in agreement with other previous works [20,30].

The titania crystallite size values, D_{200} were computed using Rigaku PDXL software based on the Scherer equation. The crystallite dimension generally increases with the titania content except the values recorded for Ti10SBA-15 and Ti20SBA-15, which are very close (Table 1).

The FTIR spectra of silica and silica–titania composites (Fig. 2) show the vibration characteristics for the inorganic matrix: the asymmetric and symmetric stretching vibrations at 1085 and 800 cm^{-1}, respectively, assigned to Si–O–Si bonds, the bands of silanol groups overlapped with Si–O–Ti vibration at 960 cm^{-1}, and the bending vibrations of Si–O bond superimposed with the band of Ti–O bond at 460 cm^{-1}. The absence of structure-directing agent bands evidences its complete removal by calcination.

The electron microscopy images of titania–silica supports revealed the formation of fiber or rope-like aggregate characteristics for SBA-15 materials, with a certain degree of ordering (straighter and longer fibers) for Ti10SBA-15 powder (Fig. 3b). The fiber-like arrangement appears more distorted with the increase in the titanium content. The EDX elemental mapping shows an even distribution of titanium in the silica framework for all titania–silica

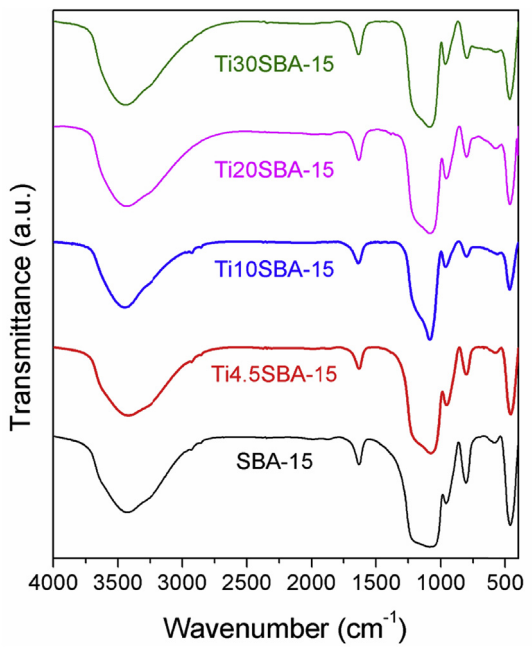

Fig. 2. FTIR spectra of SBA-15–type supports.

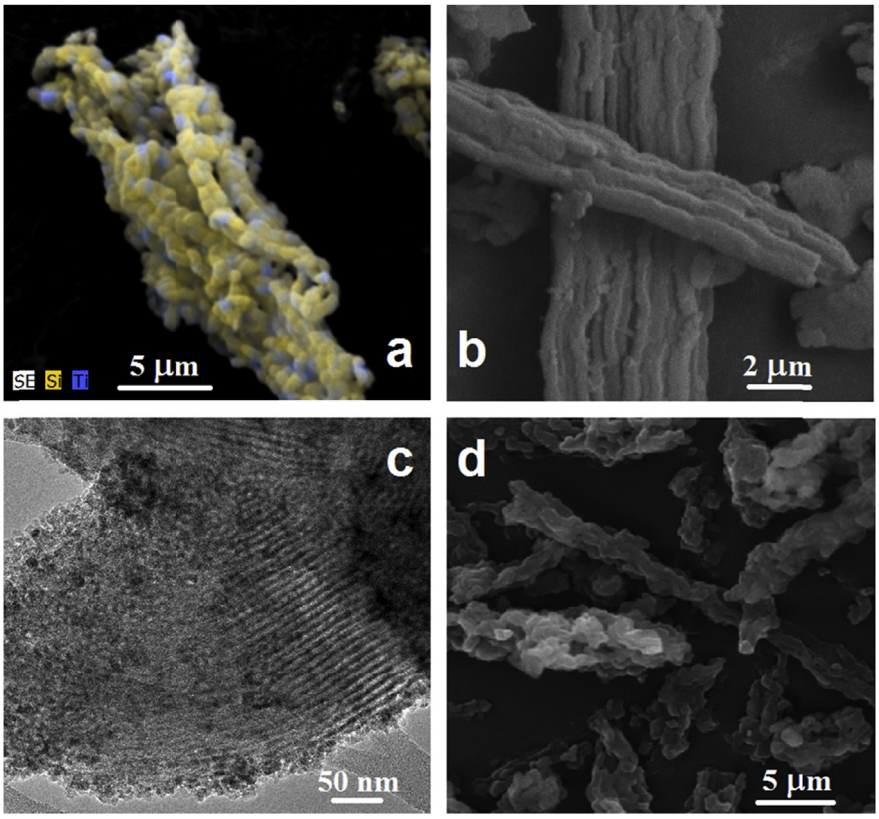

Fig. 3. Electron microscopy images of titania–silica supports: (a) SEM image of Ti4.5SBA-15 sample with EDX elemental mapping; (b) SEM image of Ti10SBA-15; (c) TEM image of Ti20SBA-15 sample; and (d) SEM image of Ti30SBA-15 samples.

samples (Fig. 3a and Fig. S1), whereas crystalline titania nanoparticles are noticed in both SEM and TEM images (Fig. 3b–d).

All samples present type IV N_2 adsorption/desorption isotherms with hysteresis, characteristic for SBA-15–type materials (Fig. 4a), and unimodal pore size distribution curves (Fig. 4b). Larger pore size values were obtained for pristine SBA-15 than for titania–silica samples (Table 1) suggesting a contraction of the mesoporous framework due to the presence of the titanium dopant. Although a slight increase in the pore size is noticed with increasing titania content, the wall thickness values remains relatively constant, indicating the saturation of the mesostructure in titanium. Notably, the textural properties of the Ti10SBA-15

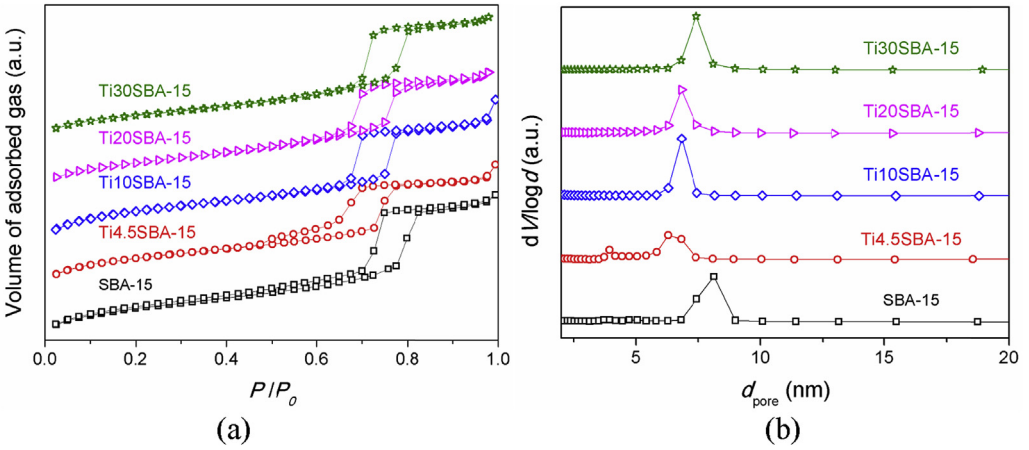

Fig. 4. Nitrogen adsorption/desorption isotherms of supports (a) and their corresponding pore size distribution curves (b).

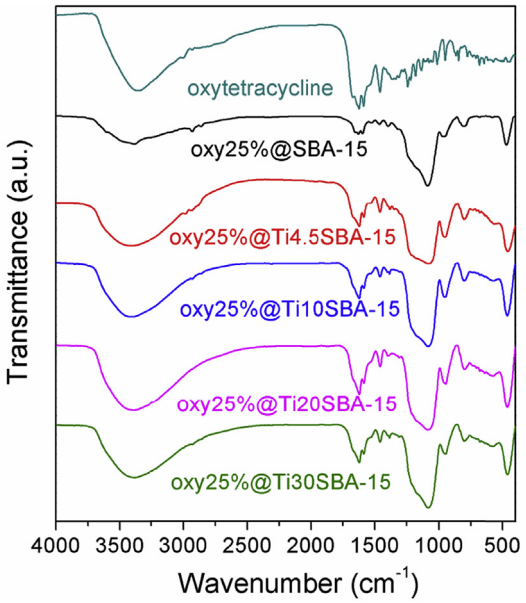

Fig. 5. FTIR spectra of oxytetracycline-loaded samples.

and Ti20SBA-15 samples, as well as the titania crystallite size for both samples are similar, despite the difference in a_0 lattice parameter.

The FTIR spectra of all oxytetracycline-loaded samples (Fig. 5) evidence the presence of antibiotic into the inorganic matrices. Its characteristic vibrations are identified in the range of 2850–2950 cm^{-1}, ascribed to the methylene groups, 1590–1650 cm^{-1}, attributed to the amide groups, and 1310–1410 cm^{-1}, assigned to the phenol moieties [31]. Correlating the FTIR spectra with the wide-angle XRD patterns (Fig. 6a and b), where no diffraction peaks of the drug are present, one can conclude that the oxytetracycline molecules were adsorbed into the pores of support in the amorphous state.

Similar to the supports, all drug-loaded samples exhibit type IV N_2 adsorption/desorption isotherms, but with narrow hysteresis loop (Fig. 7) indicating that not all the pores are completely filled with drug molecules. However, the samples showed lower porosity than the corresponding carriers, more pronounced in the case of materials containing 33 wt % drug (Table 2) and reduced values for both specific surface area and total pore volume. On the other hand, the pore size values decrease for drug-loaded SBA-15 silica, whereas for the samples containing titania–silica materials remain almost unchanged. This indicates a different mechanism of the drug hosting into the support mesopores, namely, by adsorption onto the inner pore surface in the case of pristine SBA-15 and a loading that involves the pore clogging being more likely for the titanium-doped silica network. The origin of this opposite behavior could lay on the different wetting properties of silica and titania–silica materials.

3.2. Drug delivery profiles

The oxytetracycline release experiments were performed in PBS 0.2 M, pH 5.7, at 37 °C under magnetic stirring (150 rpm). The release profiles (Fig. 8) show a decrease in the antibiotic release from Ti10SBA-15, Ti20SBA-15, and Ti30SBA-15, whereas from Ti4.5SBA-15 the profiles are similar to those recorded for the drug-loaded SBA-15 samples, presenting even a higher burst effect (Fig. S2). The crystalline titania, located on the silica surface, positively contribute to the decrease in the drug delivery rate. The lowest sustained antibiotic release rates were noticed for oxy25@Ti10SBA-15 (Fig. S2a) and oxy33@Ti10SBA-15 (Fig. S2b) samples, an expected performance as the longest fiber-like structures were observed for Ti10SBA-15 support.

The experimental drug release profiles were fitted with a three-parameter theoretical kinetic model. This model assumes that there is an equilibrium between drug molecules adsorbed onto the carrier surface and desorbed molecules inside the mesopores [32–34]. The molecules are transported through the mesochannels into the release medium by diffusion, which is assumed to follow a first-order kinetics. The adsorption/desorption equilibrium is characterized by the molecular free enthalpy, ΔG, whereas

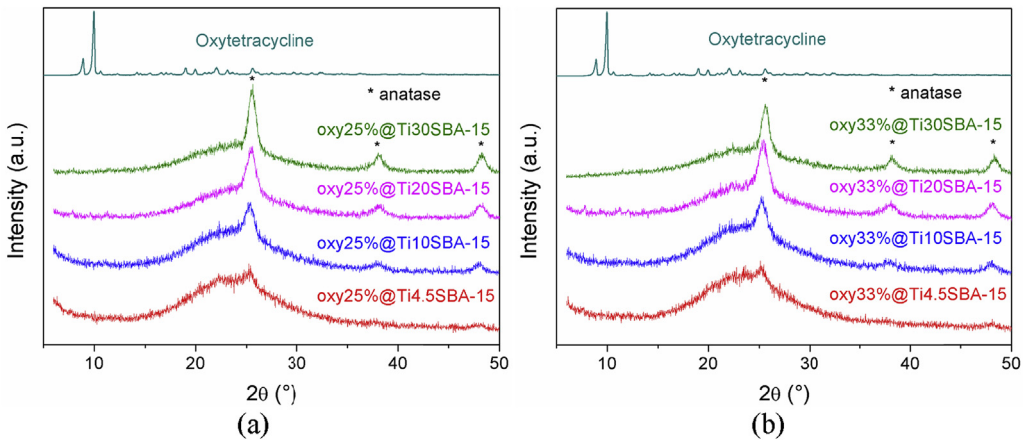

Fig. 6. Wide-angle XRD patterns of oxytetracycline-loaded samples with (a) 25 wt % and (b) 33 wt % oxytetracycline.

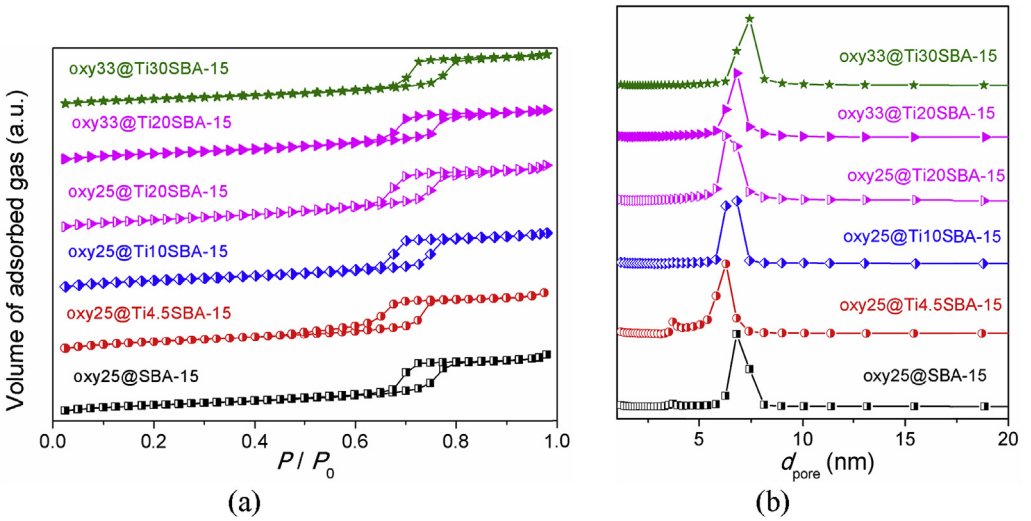

Fig. 7. Nitrogen adsorption/desorption isotherms of representative oxytetracycline-loaded samples (a) and their pore size distribution curves (b).

Table 2
Textural properties of oxytetracycline-loaded supports.

Samples	S_{BET} (m^2/g)	d_{BJH}[a] (nm)	V_{pt}/V_p[b] (cm^3/g)
oxy25%@SBA-15	302	6.81	0.5/0.57
oxy25%@Ti4.5SBA-15	333	6.29	0.56/0.51
oxy25%@Ti10SBA-15	337	6.30	0.53/0.48
oxy25%@Ti20SBA-15	353	6.29	0.63/0.57
oxy25%@Ti30SBA-15	314	6.81	0.61/0.68
oxy33%@SBA-15	208	6.28	0.34/0.37
oxy33%@Ti4.5SBA-15	219	6.28	0.36/0.44
oxy33%@Ti10SBA-15	327	6.29	0.48/0.56
oxy33%@Ti20SBA-15	284	6.82	0.47/0.51
oxy33%@Ti30SBA-15	233	7.43	0.45/0.49

[a] Pore diameter determined from the desorption branch of isotherm.
[b] V_{pt}/V_p is the total pore volume including mesopores and macropores versus pore volume calculated for pores with diameter up to 10 nm.

the rate constant for the transport process is denoted as k_d. The free enthalpy, ΔG, is directly proportional to the drug fraction released in the first, fast stage of the release process. In this initial "burst" release stage, the dissociated molecules are rapidly transported into the release medium. The release rate is therefore proportional to the transport rate constant, k_d (see Supplementary Information). The values obtained for the kinetic parameters and coefficient of determination R^2 are presented in Table 3. Good R^2 values were obtained in all cases, denoting that the model can explain the experimental data. The ΔG parameter has the highest value for oxytetracycline-loaded Ti4.5SBA-15 samples, followed by drug-loaded SBA-15 materials. Increasing the titanium content over 10 mol % leads to a decrease in free enthalpy values for both 25% and 33% drug loadings. The oxytetracycline adsorption is thus favored at a higher titania content. Keeping in mind that the titanium is mainly present as a dopant in the silica framework for the

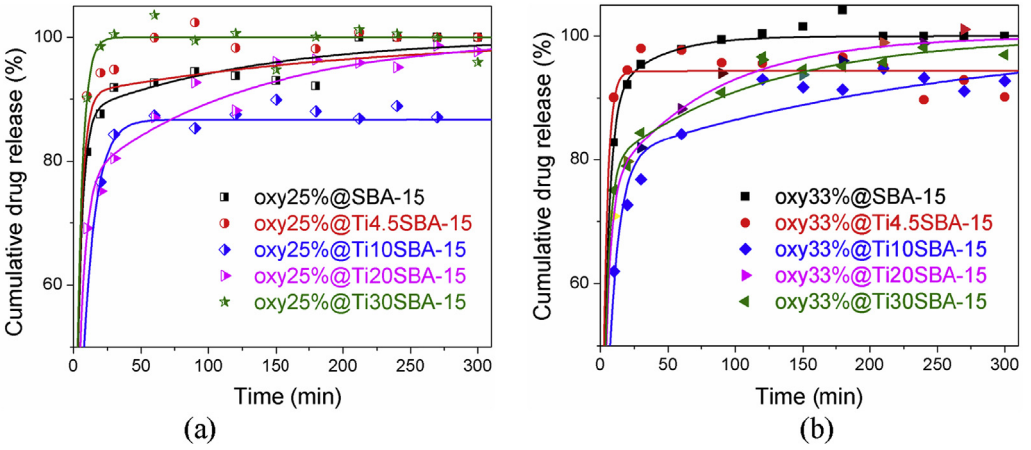

Fig. 8. Oxytetracycline release profiles for samples containing (a) 25 wt % drug and (b) 33 wt % drug. Symbols and continuous lines denote experimental and fitted data, respectively.

Table 3
Kinetic release parameters for oxytetracycline-loaded samples.

Sample	25 wt % oxy			33 wt % oxy		
	ΔG ($\times 10^{21}$ J)	k_d (min^{-1})	R^2	ΔG ($\times 10^{21}$ J)	k_d (min^{-1})	R^2
SBA-15	8.67	0.249	0.994	10.08	0.228	0.998
Ti4.5SBA-15	9.95	0.257	0.987	12.05	0.293	0.990
Ti10SBA-15	8.03	0.110	0.997	6.25	0.131	0.985
Ti20SBA-15	5.43	0.203	0.982	5.17	0.242	0.995
Ti30SBA-15	6.26	0.086	0.990	5.90	0.262	0.987

Table 4
Correlation coefficients between the carrier textural and structural parameters and the drug release kinetic parameters.

Parameters	Ti content	a_0	Wt	S_{BET}	d_{BJH}	V_p
a_0	**0.99**	1.0				
ΔG, 33% oxy	**−0.77**	**−0.81**	−0.30	0.41	−0.07	−0.25
k_d, 33% oxy	0.14	0.12	0.16	−0.62	−0.12	−0.67
ΔG, 25% oxy	**−0.83**	**−0.88**	−0.26	0.69	−0.15	−0.13
k_d, 25% oxy	−0.72	−0.69	−0.27	0.27	−0.03	0.20

For convenience, the largest correlation coefficients are in bold.

Ti4.5SBA-15 carrier, the ΔG decrease implies that drug adsorption is favored by the presence of the crystalline anatase phase. A lower drug loading (25%) leads to a decrease in the free enthalpy parameter in comparison to the sample with a higher antibiotic content. This effect can be easily understood based on steric crowding of the mesopore surface and volume. The samples with a higher drug loading have a smaller fraction of oxytetracycline molecules adsorbed onto the carrier pore wall surface, shifting the equilibrium toward desorption.

The diffusion rate k_d follows the same trend as the ΔG parameter with respect to the titanium content. In this case, the presence of crystalline TiO_2 nanoparticles inside the mesopores hinders the drug diffusion for the Ti10SBA-15, Ti20SBA-15, and Ti30SBA-15–containing samples. There are no major differences between the rate constants at different drug loadings at the same titanium content, indicating that the drug transport process is not significantly affected by the antibiotic loading amount.

A correlation study between the kinetic release parameters and the textural properties of the carriers has been considered (Table 4). The correlation coefficients take values between −1 and 1, with values close to ±1 denoting either direct or inverse correlation and values close to 0 indicating no correlation. The results show that titanium content is strongly correlated with the unit cell parameter (a_0) of mesophase. These two parameters also show an inverse correlation with the free enthalpy ΔG for both 25% and 33% drug loadings. Thus increasing the titanium content is a promising strategy to design controlled oxytetracycline delivery systems.

3.3. Antimicrobial activity of drug-loaded samples

The antimicrobial activity of oxytetracycline-containing samples with 25 wt % drug content was assessed against Gram-positive *S. aureus ATCC 25923*, Gram-negative *E. coli* ATCC 25922, and *P. aeruginosa* strains. After 24 h of incubation, all prepared samples demonstrated good and similar bactericidal activity (Fig. 9). The best antimicrobial activity was observed against *S. aureus* strain. The measured growth inhibition zone diameters for tested antibiotic-loaded samples were 34 ± 2 mm versus 36 ± 1 mm of the positive control for *S. aureus*, 30 ± 2 mm

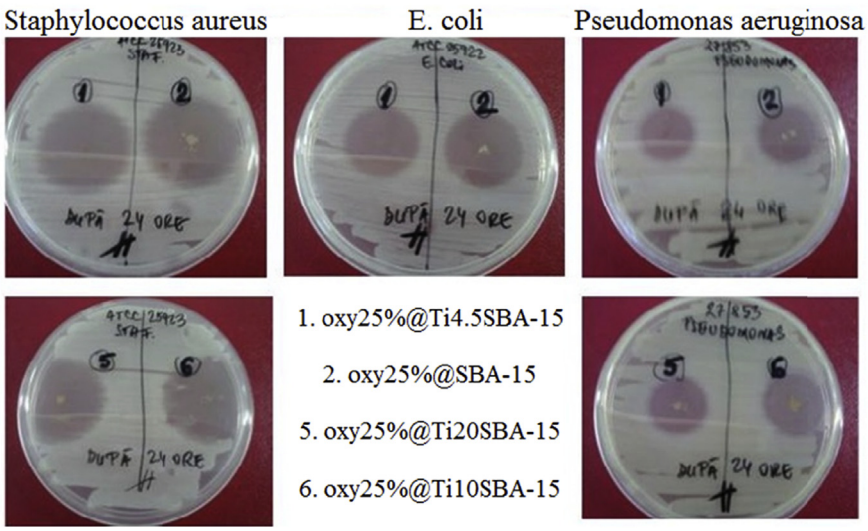

Fig. 9. Assay for determination of the growth inhibition zone diameters after 24 h of incubation for tested drug-loaded samples.

versus 32 ± 2 mm for antibiotic in the case of *E. coli*, and 21 ± 2 mm versus 22 ± 1 mm of control for *P. aeruginosa* strain.

4. Conclusions

Mesoporous titania–silica composites were successfully synthesized in the presence of Pluronic P123, with titanium content up to 30 mol %, exhibiting an ordered hexagonal pore array specific to SBA-15–type materials and high porosity, properties required for a carrier in drug delivery systems. The silanol groups on the pore wall surface of SBA-15 silica can weakly interact with oxytetracycline through hydrogen bonds that are not strong enough to keep the antibiotic molecules into mesostructured silica channels. The presence of titania nanoparticles on the silica surface can create stronger host–guest interactions between the support and oxytetracycline molecules because of donor–acceptor bond formation in which titanium ions are involved. Doping the silica network with titanium ions modified the structural and pore surface properties of support, inducing a burst effect in the first stage of oxytetracycline delivery profiles, whereas the presence of the crystalline anatase on the silica surface contribute to a sustained drug release in the last stage, both altering the release mechanism. Thereby controlling the distribution and content of titanium between the silica network and anatase phase is a promising strategy to develop oxytetracycline delivery systems with desired drug release profile, without affecting the bactericidal activity. All tested oxytetracycline-loaded samples showed a good antimicrobial activity against *S. aureus ATCC 25923*, similar to that of the antibiotic alone.

Appendix A. Supplementary data

Supplementary data related to this article can be found at https://doi.org/10.1016/j.crci.2017.09.006.

References

[1] H. Qu, S. Bhattacharyya, P. Ducheyne, Adv. Drug Deliv. Rev. 94 (2015) 96.
[2] P. Yang, S. Gai, J. Lin, Chem. Soc. Rev. 41 (2012) 3679.
[3] A. Baeza, M. Vallet-Regí, Curr. Drug Targets 17 (2016), https://doi.org/10.2174/1389450117666160603023037.
[4] D. Edeler, M.R. Kaluđerović, B. Dojčinović, H. Schmidt, G.N. Kaluđerović, RSC Adv. 6 (2016) 111031.
[5] D. Berger, L. Bajenaru, S. Nastase, R.A. Mitran, C. Munteanu, C. Matei, Micropor. Mesopor. Mater. 206 (2015) 150.
[6] R. Diab, N. Canilho, Adv. Coll. Interface Sci. (2017), https://doi.org/10.1016/j.cis.2017.04.005, in press.
[7] M. Petrescu, R.A. Mitran, A.M. Luchian, C. Matei, D. Berger, UPB Sci. Bull., Ser. B 77 (2015) 13.
[8] E. Ghenadi, V. Nichele, M. Signoretto, G. Cerrato, Chem. Eur. J. 18 (2012) 10653.
[9] S. Atefyekta, B. Ercan, J. Karlsson, E. Taylor, S. Chung, T.J. Webster, M. Andersson, Int. J. Nanomedicine 11 (2016) 977–990.
[10] J. Karlsson, A. Martinelli, H.M. Fathali, J. Bielecki, M. Andersson, J. Biomed. Mater. Res., Part A 104A (2016) 620–629.
[11] A. Datta, S. Dasgupta, S. Mukherjee, J. Nanopart. Res. 19 (2017) 142.
[12] A. Mehta, A. Mishra, M. Sharma, S. Singh, S. Basu, J. Nanoparticle Res. 18 (2016). Article number 209.
[13] Y. Yu, M. Zhu, W. Liang, S. Rhodes, J. Fang, RSC Adv. 5 (2015) 72437.
[14] Y. Na Kim, G.N. Shao, S.J. Jeon, S.M. Imran, P.B. Sarawade, H.T. Kim, Chem. Eng. J. 231 (2013) 502.
[15] N. Guo, Y. Liang, S. Lan, L. Liu, G. Ji, S. Gan, H. Zou, X. Xu, Appl. Surf. Sci. 305 (2014) 562.
[16] S.F. Resende, E.H.M. Nunes, M. Houmard, W.L. Vasconcelos, J. Colloid Interface Sci. 433 (2014) 211.
[17] K. Shiba, T. Takei, M. Ogawa, Dalton Trans. 45 (2016) 18742.
[18] N.B. Lihitkar, M.K. Abyaneh, V. Samuel, R. Pasricha, S.W. Gosavi, S.K. Kulkarni, J. Colloid Interface Sci. 314 (2007) 310.
[19] G. Zaccariello, E. Moretti, L. Storaro, P. Riello, P. Canton, V. Gombac, T. Montini, E. Rodriguez-Castellone, A. Benedetti, RSC Adv. 4 (2014) 37826.
[20] M.M. Wan, X.D. Sun, S. Liu, J. Ma, J.H. Zhu, Microporous Mesoporous Mater. 199 (2014) 40.
[21] S. Bhattacharyya, A. Agrawal, C. Knabe, P. Ducheyne, Biomaterials 35 (2014) 509.
[22] M.B.M. Al Tameemi, R. Stan, V. Prisacari, G. Voicu, M. Popa, M.C. Chifiriuc, C. Ott, G. Marton, A. Meghea, C. R. Chimie 20 (2017) 475.
[23] S. Hashemikia, N. Hemmatinejad, E. Ahmadi, M. Montazer, J. Colloid Interface Sci. 443 (2015) 105–114, https://doi.org/10.1016/j.jcis.2014.11.020.
[24] D. Mishra, P. Khare, K. Shanker, D.K. Singh, S. Luqman, New Horizons Transl. Med. 3 (2016) 66–72.
[25] B.S. Mithila, N.R. Ravikumara, B. Madhusudhan, J. Bionanosci 7 (2013) 403–414.
[26] S.A. Kleinubing, D.C. Seraphim, M.G. Adeodato Vieira, R.L.S. Canevesi, E.A. da Silva, C.L. Cesar, L.H. Innocentini Mei, J. Appl. Polym. Sci. (2014), https://doi.org/10.1002/APP.40444.
[27] D. Berger, S. Nastase, R.A. Mitran, M. Petrescu, E. Vasile, C. Matei, T. Negreanu-Pirjol, Int. J. Pharm. 510 (2016) 524.
[28] M. Petrescu, R.A. Mitran, C. Matei, D. Berger, Rev. Roum. Chim. 61 (2016) 557.
[29] S.Y. Chen, T. Mochizuki, Y. Abe, M. Toba, Y. Yoshimura, Appl. Catal., B Environ. 344 (2014) 148–149.
[30] L. Yang, Z. Jiang, S. Lai, C. Jiang, H. Zhon, Int. J. Chem. Eng. (2014), https://doi.org/10.1155/2014/691562, Article ID 691562, 7 pages.
[31] G. Socrates, Infrared and Raman Characteristic Group Frequencies: Tables and Charts, 3rd ed., John Wiley and Sons, Chichester, UK, 2001.
[32] L. Zeng, L. An, X. Wu, J. Drug Deliv. 370308 (2011) 15.
[33] M. Martínez-Carmona, M. Colilla, M.L. Ruiz-González, J.M. González-Calbet, M. Vallet-Regí, Microporous Mesoporous Mater. 225 (2016) 399.
[34] R.A. Mitran, C. Matei, D. Berger, J. Phys. Chem. C 120 (2016) 29202.